This is the Pre-Published Version.

This document is the Accepted Manuscript version of a Published Work that appeared in final form in ACS Nano, © 2023 American Chemical Society after peer review and technical editing by the publisher. To access the final edited and published work see https://dx.doi.org/10.1021/acsnano.3c01919.

Charge-powered electrotaxis for versatile droplet manipulation

Yuankai Jin[1], Xiaonan Liu[1], Wanghuai Xu[2], Pengcheng Sun[1], Siping Huang[3], Siyan Yang[1], Xiao Yang[1], Qinggong Wang[4], Raymond H. W. Lam[3], Ruirui Li[5,*], and Zuankai Wang[2,*]

[1]Department of Mechanical Engineering, City University of Hong Kong, Hong Kong, 999077, P.R. China.

[2]Department of Mechanical Engineering, The Hong Kong Polytechnic University, Hong Kong, 999077, P.R. China.

[3]Department of Biomedical Engineering, City University of Hong Kong, Hong Kong, 999077, P.R. China

[4]Qian Xuesen Laboratory of Space Technology, China Academy of Space Technology, Beijing, 100094, P.R. China

[5]State Key Laboratory of Dynamic Measurement Technology, North University of China, Taiyuan, 030051, P.R. China

*Ruirui Li, Zuankai Wang

Email:liruirui@nuc.edu.cn; zk.wang@polyu.edu.hk

ToC

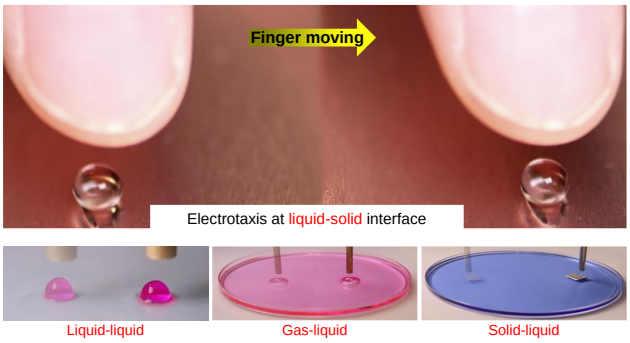

ABSTRACT. Taxis is an instinctive behavior of living organisms to external dangers or benefits. Here, we report a taxis-like behavior associated with liquid droplets on charged substrates in response to the external stimuli, referred to as droplet electrotaxis. Such droplet electrotaxis enables us to use either solid or liquid (such as water) matter, even human finger, as stimuli to spatiotemporal-precisely manipulate the liquid droplets of various physicochemical properties, including water, ethanol with low surface tension, viscous oil, and so on. Droplet electrotaxis also features a flexible configuration, that even can manifest in the presence of an additional layer, such as the ceramic with a thickness of ~ 10 mm. More importantly, superior to existing electricity-based strategies, droplet electrotaxis can harness the charges generated from diverse manners, including pyroelectricity, triboelectricity, piezoelectricity, and so on. These properties dramatically increase the application scenarios of droplet electrotaxis, such as cell labeling and droplet information recording.

KEYWORDS: electrotaxis, droplet manipulation, interface, taxis, charge.

Introduction

Taxis is the directional and preferential movement of active matter in response to external stimuli, which is widely manifested in the natural world. In particular, the taxis of living organisms endows

them to survive and evolve in resource-limited settings. Less apparent is that taxis can also be manifested in artificial systems.[1-4] A typical application scenario of artificial taxis is droplet manipulation; for example, a recently reported durotaxis, referred to as the taxis motion directed by the stiffness gradients of the underlying substrate[5], can effectively drive the directional motion of droplets.[6-8] However, such durotaxis-enabled droplet manipulation is limited by the poor controllability for droplet motion because the durotaxis is passively triggered by the pre-determined substrate properties. Accordingly, introducing the external force source, such as electricity, to actively evoke the taxis property of droplets might be a more promising means for droplet manipulation. Various electricity-based strategies, such as electrowetting,[9, 10] electro-dewetting,[11] dielectrophoresis,[12-14] surface charge printing,[15, 16] Coulomb attraction/repulsion,[17-21] and so on,[22-28] have been widely used in droplet manipulation. Despite great improvement in droplet manipulating performance, these methods still suffer from several limitations, such as the complexity of the manipulation platform, instability of droplet motion, and so on.

Here, we report that the charge-powered droplet shows electrotaxis in response to external stimuli, which offers us a flexible yet powerful tool for droplet manipulation. Such droplet electrotaxis is generic to diverse interfaces, such as liquid-solid interface, liquid-liquid interface, gas-liquid interface, and so on. Superior to the conventional designs, the droplet electrotaxis decouples energy-supplying and motion-controlling functions, which dramatically increases its adaptability for various stimulus materials and charge sources, such as pyroelectricity, triboelectricity, piezoelectricity, and so on. We also demonstrate that droplet electrotaxis can be harnessed in various droplet-related applications such as cell treatments and droplet information recording.

Results and Discussion

Figure 1A shows a representative droplet electrotaxis, in which a water droplet on an electrostatically charged superhydrophobic surface moves following the human finger (Movie S1). Such a contactless finger-guided droplet electrotaxis shows a facile and precise control for droplet motion, which is dramatically different from some existing works where the finger cannot regulate the droplet motion.[29, 30] Figure 1B sketches out the three key elements to achieve droplet electrotaxis, including droplet, charged substrate, and contactless external stimulus (such as human fingers). Here, the stimulus, a term in the taxis, can also be understood as a counter electrode from the perspective of the electric circuit. The electrotaxis induces the droplet to bead up toward the

stimulus (Figure 1B and Figure S1A), which is totally contrary to electrowetting where the droplet tends to spread on substrates. In addition, different from electrowetting necessitating an ultrathin dielectric layer (at the scale of micrometers),[31] droplet electrotaxis manifests in the situations of both the presence and absence of an additional dielectric layer, and the thickness of the dielectric layer for droplet electrotaxis can be even at a millimeter scale, demonstrating its flexible configuration. Figure 1C and Movie S2 show the electrotaxis motion of the water droplet on a copper-supported dielectric alumina ceramic layer (with a thickness of 10 mm) in response to the stimulation from a shape-regular cylindrical copper rod. In addition to the dielectric ceramic, other materials, such as polymers, can also serve as the additional layer to support the electrotaxis motion of droplet (Figure S2A). We also find that the additional dielectric layer imposes a very weak influence on the droplet electrotaxis, which is verified by comparing the contact angles of droplets without the dielectric layer and with 10 mm of dielectric ceramic layer (Figure 1D). Figure 1D also suggests that the droplet electrotaxis is regulated by the electrostatic voltage on charged substrates, which is further discussed in Figure S3.

Droplet electrotaxis originates from the electrostatic attraction between droplet and external stimuli, which is discussed in NOTE S1 in detail. Briefly, taking the positively charged substrate as an example, the substrate can instantaneously conduct the partial positive charges into the droplets (Figure 2A), which is a process of charge redistribution,[32, 33] and the magnitude of droplet charges is proportional to that of the substrates (Figure S4A, B), Notably, droplet charges always keep stable during its motion (Figure S4C), which could eliminate the possible manipulation instability caused by the undesirable triboelectrification during droplet moving on substrate.[15, 17] Next, the positive charges in droplets and substrates result in the generation of negative induced charges in the stimulus rod due to the electrostatic induction.[33,34] Consequently, the opposite polarity of charges in droplet and stimulus rod results in the attractive electrostatic force acting on the droplet. For the situation of negatively charged substrates, the electrostatic force still exists because the droplet and stimulus rod could acquire negative and positive charges, respectively, demonstrating the independence of droplet electrotaxis on the charge polarity. The interaction between the droplet and stimulus rod could also be understood by resorting to the simulation method (finite-element analysis using the COMSOL-Multiphysics simulation). Figure 2B and the inset show the electric potential distribution of the whole droplet electrotaxis system and the

Maxwell stress tensor of the droplet, respectively, both of which illustrate that droplet is subjected to an electrostatic force pointing to the external stimulus.

The above analysis reveals that for droplet electrotaxis, the charged substrates and external stimuli implement the energy-supplying and motion-controlling functions, respectively, suggesting a functional-decoupling property. Such a property dramatically eliminates the overall complexity of droplet electrotaxis in comparison to the traditional electricity-based droplet control strategies in which droplet motion is simultaneously powered and controlled by the sophisticated electric circuit or movable electrodes.[9-13, 19] Therefore, we can use the stimulation from not only solid matter made of different materials, but also liquid matter to trigger the droplet electrotaxis. And the capability of the different solid stimuli can be quantitatively evaluated by the voltage range for the droplet electrotaxis motion (left part of Figure 2C). We find that copper, carbon, and wood rod possess almost the same capability in stimulating droplet electrotaxis. However, ceramic rod with low electric conductivity needs a higher voltage range for droplet electrotaxis motion. In contrast, insulated polymeric rods, including acrylonitrile butadiene styrene (ABS) and polyoxymethylene (POM), cannot activate the droplet electrotaxis regardless of the applied voltages because the weak electric responsiveness of these materials leads to less induced charges and accompanied weaker electrostatic attraction toward the droplet (Figure S5). Based on such an understanding, we can also use the liquid stimulus to trigger the droplet electrotaxis. Figure 2C (right part) and Movie S3 show that the water (blue colored) filled in a pipette could evoke the electrotaxis motion of a water droplet (red colored), but the empty pipette without water cannot trigger the droplet motion (Figure S6).

The droplet electrotaxis allows us to manipulate the droplet in a precise and flexible manner, which profits from the remote and spatiotemporal properties of the electrostatic force between the droplet and external stimulus. As shown in Figures 2D, E and Movie S4, we can maneuver the water droplet (~7 μL) to travel along circle tracks with diameters of 5 mm and 20 mm, respectively, demonstrating a precise control for the droplet motion track. Note that such a dexterous droplet manipulation is hard to be achieved in traditional electrowetting-based droplet manipulation where pre-designed and orderly-arranged electrode patterns limit either sharp or circular directional change of droplet motion. In addition to the single droplet, droplet electrotaxis also allows for the manipulation of the droplet array. Figure 2F and Movie S5 show the electrotaxis motion of droplet

arrays comprising four water droplets under the stimulation of four metal rods, and Figure S7 shows a single manipulator can also simultaneously manipulate four water droplets. Such alternative strategies for collective electrotaxis of droplet array offer a promising platform for applications that need high-throughput droplet transport. Furthermore, the electrotaxis-enabled droplet manipulation possesses other aspects of merits, such as the wide droplet volume range (from the scale of 10^{-1} to 10^{3} μL, Figure S8), high moving velocity (upper limiting speed in our experimental conditions, ~ 203 mm/s, Figure S9), and so on.

Electrotaxis is a universal property for various liquid droplets with different physicochemical features. Theoretically speaking, all the charged droplets could show electrotaxis. And a previous study has proven that even insulating nonpolar organic liquids can obtain charges from charged substrates.[35] Here, we demonstrate the electrotaxis motion of four liquids, including water, ethanol, surfactant (10 wt.% sodium dodecyl sulfate aqueous solution), and oil, on the lubricant-infused slippery surfaces (Figure 3A and Movie S6), and the magnitude of charges in these liquids is shown in Figure S10. Here, using a lubricant-infused slippery surface, as an alternative to the superhydrophobic surface, forms a preferential liquid-liquid interface,[35-38] which endows a favorably stable lyophobicity and low surface resistance (Table S1) to the liquid droplets with a wide range of surface tensions and viscosities. Similarly, we can also resort to the liquid substrates, that is charged by a short-time contact with the power supply (Figure S11), to form the low-resistance gas-liquid and solid-liquid interface, thereby achieving the electrotaxis of the gas bubble (Figure 3B, Movie S7) and solid raft (Figure 3C, Movie S8), respectively. Here, the bubble and solid raft are subjected to a low resistance due to the low velocity (~ 0.7 cm/s) and low viscosity of the liquid. Note that manipulation for gas bubbles and solid objects is critical for many applications, such as the purification of polluted air with particulate matter.[39] In addition, the droplet electrotaxis is also applicable to the water droplet under oil[40], a liquid-solid interface in the liquid medium (Figure S2B). We can conclude that, from the interfacial perspective between droplets and substrates, the droplet electrotaxis is generic to various droplet-substrate interfaces that are listed in Figure 3D.

Another merit of droplet electrotaxis is its wide adaptability to various sources of electrostatic charges that are even randomly distributed. In addition to the above-used electrostatic power supply, we can also use diverse charge sources, such as pyroelectricity, triboelectricity, and so on,

to energize the droplet electrotaxis, which is also a benefit of function-decoupling property. Figure 4A shows the design of pyroelectricity-powered droplet electrotaxis. Such a design mainly relies on pyroelectric materials, such as lithium niobate crystal $LiNbO_3$ that can generate surface charges from temperature variation,[41] and the conductive layer between droplet and $LiNbO_3$ crystal can prevent the undesired furcated motility of droplet[42, 43]. Taking room temperature (~28 ^oC) as an initial temperature, the temperature increases and decreases result in the generation of negative and positive voltage, respectively (Figure 4B). When the surface temperatures change to ~21 ^oC or ~36 ^oC, the generated charges can drive the electrotaxis motion of droplet, as shown in the infrared picture in Figure 4C and Movie S9.

Figures 4D-F show the triboelectricity-powered droplet electrotaxis. As a demonstration, we chose plastic petri dishes to generate and store triboelectric charges due to their easy availability and strong electronegativity.[44] Being rubbed with other matters, the petri dish surface generates randomly distributed electrostatic charges (illustrated in Figure 4D), which can form uniform surface voltage in the presence of a conductive copper sheet due to the equipotential property of metal copper. The generated voltage on the copper surface is at the scale of several kilovolts (~ -3 kV, Figure 4E), which is enough to power the droplet electrotaxis motion (Figure 4F and Movie S10). Note that if the conductive substrate is absent, the randomly distributed surface charges on the petri dish will lead to an unpredictable and uncontrollable droplet motion (Figure S12, Movie S11), meaning the failure of electrotaxis.

In addition to pyroelectricity and triboelectricity, other kinds of manners to generate electrostatic charges, such as corona discharge (Figure S13), electrostatic induction (Figure S14), piezoelectricity, and so on, are also available to power the droplet electrotaxis. And as a demonstration, we use a video (Movie S12) to introduce how to use the electrostatic charges generated from the piezoelectric device in the lighter to power the droplet electrotaxis.

Electrotaxis-enabled precise and flexible droplet manipulation can be harnessed for many practical applications in various fields. Here, we demonstrate the applications of droplet electrotaxis in cell labeling and droplet information recording, both of which are based on the fact that the droplet is a good carrier for the substances and information. To accomplish cell labeling, we designed an enclosed droplet electrotaxis system that takes a disposable petri dish, the most common cell culture plate found in biomedical laboratories, as the skeleton (illustrated in Figure 5A). Such an

enclosed droplet electrotaxis system offers a low-cost, contactless, high-controllable, and portable manner for the moving (Figure 5B) and merging (Movie S13) of the droplets that are isolated from the outside environments. As a demonstration, we manipulated the droplet containing the cells in such an enclosed electrotaxis system to merge with the droplet containing Hochest and the droplet containing Dil to stain the nucleus and membrane of cells, respectively, and labeled results are tested by the fluorescence images (Figure 5C). Additionally, the enclosed system with the skeleton of petri dish can also provide a pollution-free cell culture environment, which is crucial for some cell staining scenarios, and one typical example is the proliferation analysis of cells dyed by carboxyfluorescein succinimidyl ester[45]. Furthermore, such an enclosed electrotaxis system also allows for the integration of more functions, for example, adding gas inlets and outlets to control the gaseous environment for the cell culture.

To record the droplet information, we select three types of sensors to detect the temperature, color, and capacitance of the droplet during its electrotaxis motion (Figure 5D). As an illustration, we first manipulated a water droplet (~16 μL) to dissolve sodium hydroxide (~ 8 mg), and the temperature sensor recorded the droplet temperature change (Figure 5E). Next, the as-reacted alkaline liquid droplet was moved to merge with the dilute phenolphthalein droplet (8 μL), causing the color change of the droplet from transparency (recorded as white) to pink, and such a color change is reflected by the RGB (red, green, blue) values detected by the color sensor (Figure 5F). Further, the droplet was moved to the declivous interdigital electrode that serves as the capacitive sensor, which forms a counting peak (Figure 5G). In fact, such a capacitive sensor can also be used to record other information of the droplets, such as concentration, size, and so on.[46]

Conclusion

In analog to the taxis properties of natural lives, abiotic droplets on charged substrates also undergo a taxis behavior toward the external stimulus, termed droplet electrotaxis. The droplet electrotaxis demonstrates a generality in the selection of droplets, substrates, and stimuli, as well as a strong adaptability in charge sources generated in various manners, which provides droplet manipulation with simplicity, versatility, and flexibility. Further combining the capability of droplets in dealing with both biotic and abiotic information and substance, droplet electrotaxis can serve as a promising tool for diverse applications in a wide range of fields, such as cell staining and droplet information detection.

Materials and Methods

Surface processing

To render copper, ceramic, ITO surface, petri dish, the interdigital electrode of the capacitive sensor, and other polymer surfaces with superhydrophobicity, these surfaces were first sprayed using a commercial superhydrophobic sprayer, Glaco (purchased from Soft99 Corporation), followed by heating at 60 ºC for 5 minutes. The lubricant-infused slippery surface was obtained by dripping the oil (DuPont Krytox GPL 10) on the porous PTFE membrane supported by the alumina. To enhance the stability PTFE membrane on aluminum, PTFE was wetted with ethanol and then naturally dried before oil dripping. The ITO coating on the inner bottom surface of the plastic petri dish (with a thickness of ~30 nm) was coated by a dual-target sputtering system (Q150TS, Quorum). Bubbles were generated by injecting the air into SDS aqueous solution using a syringe.

The phenolphthalein indicator (1 wt.% in ethanol, Aladdin) solution was firstly volatilized to 20 % of the initial volume by heating to 50 ºC, and then diluted by deionized water with a volume of 15 times higher than that of concentrated phenolphthalein solution. Such a dilute process allows the substrate to be superhydrophobic to the phenolphthalein indicator. SDS (sodium dodecyl sulfate, Sigma-Aldrich) and silicon oil (with a viscosity of ~10 mPa s, Aladdin) were directly used without further purification.

Cell culture and labeling

HL-60 cells were firstly seeded in Dulbecco's modified eagle medium at 37 ºC for 24 hours. Then, the droplet containing cells was transferred to the enclosed electrotaxis system, and then manipulated to merge with the PBS aqueous droplet with 1 μg/mL of Hochest, achieving the staining of the cell nucleus. After that, the reacted droplet was further manipulated to merge with the PBS aqueous droplet containing 1 μg/mL of Dil, achieving the labeling of the cell membrane. Finally, the droplet was deposited on a glass microscope slide for fluorescence imaging by a confocal microscope system (TCS-SP8, Leica Microsystems).

Fabrication of enclosed droplet electrotaxis system

The enclosed electrotaxis system uses a disposable petri dish, the most common cell culture plate found in biomedical laboratories, as the skeleton. The bottom inner surface of the petri dish was coated with a conductive superhydrophobic coating (ITO coating) to support the droplets, and the upper surface of the petri dish was replaced by an elastic film (PDMS film with a thickness of 100 μm), which allows us to exert stimuli on droplet by deforming the elastic film.

Instrument and characterization

The surface voltage was measured by a handheld electrostatic voltage tester (FMX-003, Xiangruide Corp.) with a resolution of ±0.01 kV. The charges in droplets on various surfaces were measured by a Faraday cup connected to a nanocoulomb meter (Monroe Electronics Model 284). The motion of the droplet, programmatically controlled by a stepper, was recorded by a high-speed camera (Fastcam SA4, Photron limited) and analyzed by using the software, ImageJ. The static and dynamic contact angles of liquids were measured by a Kruss DSA100 contact angle goniometer at ambient temperature. Infrared images were captured by an infrared camera (FLIR T1050sc). Unless specified otherwise, the substrates were charged by directly touching the output lines of the electrostatic power supply (DW-P303-1ACD1, Tianjin Dongwen High Voltage Power Supply Corp.)

ASSOCIATED CONTENT

Author Contributions

The following files are available free of charge.

Note text for the generation of electrostatic attraction in droplet electrotaxis; optical images for the droplet electrotaxis in response to the external stimulus, and schematic diagram of charge distribution during the electrotaxis; optical images for the electrotaxis of water droplet; droplet electrotaxis with various electrostatic voltage applied on the substrate; measurement of charges in the liquid droplet on charged substrates; simulated charge density distribution for droplet electrotaxis under the stimulation from conductive copper rod and insulating abs rod; optical image showing that the empty pipette without water cannot evoke the electrotaxis motion of droplets; optical images for the electrotaxis of droplet arrays in response to the motion of one manipulating

copper rod; the volume range of water droplets that can be controlled by droplet electrotaxis; optical images for the droplet traveling for ~71 mm during 0.35 s, showing a velocity of ~203 mm/s; comparison of the charges in different types of droplets (~7 μL) on the lubricant-infused slippery surface; electrotaxis on the liquid surface; water droplet motion on triboelectrified petri surface in the absence of conductive layer; corona discharge serving as the charge source of the droplet electrotaxis; induction electrification serving as the charge source of the droplet electrotaxis; dynamic contact angles of various liquids on lubricant-infused slippery surfaces (PDF)

Movie S1: Electrotaxis motion of water droplet on the superhydrophobic surface in response to the human finger (AVI)

Movie S2: Electrotaxis motion of droplet on the dielectric ceramic surface supported by the charged copper substrate (AVI)

Movie S3: Liquid stimulus (water) for the droplet electrotaxis (AVI)

Movie S4: Droplet electrotaxis motion with circular tracks (AVI)

Movie S5: Electrotaxis of droplet arrays (AVI)

Movie S6: Electrotaxis of varied liquids on the slippery surface (AVI)

Movie S7: Electrotaxis of the gas bubble on the liquid surface (AVI)

Movie S8: Electrotaxis of the solid raft on liquid surface (AVI)

Movie S9: Pyroelectricity-powered electrotaxis of droplet in low and high temperatures (AVI)

Movie S10: Droplet electrotaxis powered by triboelectric charges on the petri surface (AVI)

Movie S11: Random motion of droplet on triboelectrified superhydrophobic petri surface (AVI)

Movie S12: Piezoelectricity-powered droplet electrotaxis (AVI)

Movie S13: Enclosed droplet electrotaxis system (AVI)

Author Contributions

Y.J. and Z.W. conceived the research. Y.J. designed the experiments. Y.J. W.X. and R.L. prepared the samples. Y.J., X.L., W.X., P.S., S.H., S.Y., X.Y., Q.W., and R. L. carried out the experiments. All authors analyzed the data. Z.W. and Y.J. wrote the manuscript.

Funding Sources

We acknowledge the financial support from the National Natural Science Foundation of China (No. 51975502), Research Grants Council of Hong Kong (No. C1006-20W, No. 11213320, No. 11219219), Shenzhen Science and Technology Innovation Council (SGDX20201103093005028), the Tencent Foundation through the XPLORER PRIZE, Science and Technology Planning Project of Guangdong Province (No. 2021A0505110002).

Notes

Any additional relevant notes should be placed here.

REFERENCES

1. Qian, X.; Zhao, Y.; Alsaid, Y.; Wang, X.; Hua, M.; Galy, T.; Gopalakrishna, H.; Yang, Y.; Cui, J.; Liu, N.; Marszewski, M.; Pilon, L.; Jiang, H.; He, X., Artificial phototropism for omnidirectional tracking and harvesting of light. *Nat. Nanotechnol.* **2019,** *14*, 1048-1055.
2. Lach, S.; Yoon, S. M.; Grzybowski, B. A., Tactic, reactive, and functional droplets outside of equilibrium. *Chem. Soc. Rev.* **2016,** *45*, 4766-96.
3. Lohse, D.; Zhang, X., Physicochemical hydrodynamics of droplets out of equilibrium. *Nat. Rev. Phys.* **2020,** *2*, 426-443.
4. Lagzi, I.; Soh, S.; Wesson, P. J.; Browne, K. P.; Grzybowski, B. A., Maze solving by chemotactic droplets. *J. Am. Chem. Soc.* **2010,** *132*, 1198-9.
5. Trichet, L.; Le Digabel, J.; Hawkins, R. J.; Vedula, S. R.; Gupta, M.; Ribrault, C.; Hersen, P.; Voituriez, R.; Ladoux, B., Evidence of a large-scale mechanosensing mechanism for cellular adaptation to substrate stiffness. *Proc. Natl. Acad. Sci. U.S A.* **2012,** *109*, 6933-8.
6. Style, R. W.; Che, Y.; Park, S. J.; Weon, B. M.; Je, J. H.; Hyland, C.; German, G. K.; Power, M. P.; Wilen, L. A.; Wettlaufer, J. S.; Dufresne, E. R., Patterning droplets with durotaxis. *Proc. Natl. Acad. Sci. U.S A.* **2013,** *110*, 12541-4.
7. Bueno, J.; Bazilevs, Y.; Juanes, R.; Gomez, H., Wettability control of droplet durotaxis. *Soft Matter* **2018,** *14*, 1417-1426.

8. Kajouri, R.; Theodorakis, P. E.; Deuar, P.; Bennacer, R.; Zidek, J.; Egorov, S. A.; Milchev, A., Unidirectional Droplet Propulsion onto Gradient Brushes without External Energy Supply. *Langmuir* **2023**, 2818–2828.
9. Nie, J.; Ren, Z.; Shao, J.; Deng, C.; Xu, L.; Chen, X.; Li, M.; Wang, Z. L., Self-Powered Microfluidic Transport System Based on Triboelectric Nanogenerator and Electrowetting Technique. *ACS Nano* **2018,** *12*, 1491-1499.
10. Yi, U.-C.; Kim, C.-J., Characterization of electrowetting actuation on addressable single-side coplanar electrodes. *J. Micromech. Microeng.* **2006,** *16*, 2053.
11. Li, J.; Ha, N. S.; Liu, T.; van Dam, R. M.; cj' Kim, C. J., Ionic-surfactant-mediated electro-dewetting for digital microfluidics. *Nature* **2019,** *572*, 507-510.
12. Velev, O. D.; Prevo, B. G.; Bhatt, K. H., On-chip manipulation of free droplets. *Nature* **2003,** *426*, 515-6.
13. Liu, C.; Liu, X.; Tang, Q.; Zhou, W.; Ma, Y.; Gong, Z.; Chen, J.; Zheng, H.; Joo, S. W., Three-Dimensional Droplet Manipulation with Electrostatic Levitation. *Anal. Chem.* **2022**, *94*, 8217-8225.
14. Yang, Z.; Wei, J.; Sobolev, Y. I.; Grzybowski, B. A., Systems of mechanized and reactive droplets powered by multi-responsive surfactants. *Nature* **2018,** *553*, 313-318.
15. Sun, Q.; Wang, D.; Li, Y.; Zhang, J.; Ye, S.; Cui, J.; Chen, L.; Wang, Z.; Butt, H. J.; Vollmer, D.; Deng, X., Surface charge printing for programmed droplet transport. *Nat. Mater.* **2019,** *18*, 936-941.
16. Sun, Q.; Hu, X.; Xu, B.; Lin, S.; Deng, X.; Zhou, S., Janus Charged Droplet Manipulation Mediated by Invisible Charge Walls. *Adv. Sci.* **2022,** *9*, e2204382.
17. Dai, H.; Gao, C.; Sun, J.; Li, C.; Li, N.; Wu, L.; Dong, Z.; Jiang, L., Controllable High-Speed Electrostatic Manipulation of Water Droplets on a Superhydrophobic Surface. *Adv. Mater.* **2019,** *31*, e1905449.
18. Mertaniemi, H.; Jokinen, V.; Sainiemi, L.; Franssila, S.; Marmur, A.; Ikkala, O.; Ras, R. H., Superhydrophobic tracks for low-friction, guided transport of water droplets. *Adv. Mater.* **2011,** *23*, 2911-4.
19. Jin, Y.; Xu, W.; Zhang, H.; Li, R.; Sun, J.; Yang, S.; Liu, M.; Mao, H.; Wang, Z., Electrostatic tweezer for droplet manipulation. *Proc. Natl. Acad. Sci. U.S A.* **2022,** *119*, e2105459119.
20. Sinn, N.; Schür, M. T.; Hardt, S., No-contact electrostatic manipulation of droplets on liquid-infused surfaces: Experiments and numerical simulations. *Appl. Phys. Lett.* **2019,** *114*.
21. Tang, X.; Wang, L., Loss-Free Photo-Manipulation of Droplets by Pyroelectro-Trapping on Superhydrophobic Surfaces. *ACS Nano* **2018,** *12*, 8994-9004.
22. Li, X.; Bista, P.; Stetten, A. Z.; Bonart, H.; Schür, M. T.; Hardt, S.; Bodziony, F.; Marschall, H.; Saal, A.; Deng, X.; Berger, R.; Weber, S. A. L.; Butt, H.-J., Spontaneous charging affects the motion of sliding drops. *Nat. Phys.* **2022**.
23. Hartmann, J.; Schur, M. T.; Hardt, S., Manipulation and control of droplets on surfaces in a homogeneous electric field. *Nat. Commun.* **2022,** *13*, 289.
24. Oh, I.; Keplinger, C.; Cui, J.; Chen, J.; Whitesides, G. M.; Aizenberg, J.; Hu, Y., Dynamically Actuated Liquid‐Infused Poroelastic Film with Precise Control over Droplet Dynamics. *Adv. Funct. Mater.* **2018,** *28*, 1802632.
25. Han, X.; Tan, S.; Jin, R.; Jiang, L.; Heng, L., Noncontact Charge Shielding Knife for Liquid Microfluidics. *J. Am. Chem. Soc.* **2023,** *145*, 6420-6427.

26. Xu, W.; Jin, Y.; Li, W.; Song, Y.; Gao, S.; Zhang, B.; Wang, L.; Cui, M.; Yan, X.; Wang, Z., Triboelectric wetting for continuous droplet transport. *Sci. Adv.* **2022,** *8*, eade2085.
27. Lv, P.; Zhang, Y.; Han, D.; Sun, H., Directional droplet transport on functional surfaces with superwettabilities. *Adv. Mater. Interfaces* **2021,** *8*, 2100043.
28. Sun, X.; Feng, Y.; Wang, B.; Liu, Y.; Wu, Z.; Yang, D.; Zheng, Y.; Peng, J.; Feng, M.; Wang, D., A new method for the electrostatic manipulation of droplet movement by triboelectric nanogenerator. *Nano Energy* **2021,** *86*.
29. Peng, C.; Zhang, Z.; Kim, C. J.; Ju, Y. S., EWOD (electrowetting on dielectric) digital microfluidics powered by finger actuation. *Lab Chip* **2014,** *14*, 1117-22.
30. Sun, J.; Zhang, L.; Zhou, Y.; Li, Z.; Libanori, A.; Tang, Q.; Huang, Y.; Hu, C.; Guo, H.; Peng, Y.; Chen, J., Highly efficient liquid droplet manipulation via human-motion-induced direct charge injection. *Mater. Today* **2022,** *58*, 41-47.
31. Quilliet, C.; Berge, B., Electrowetting: a recent outbreak. *Curr. Opin. Colloid Interface Sci.* **2001,** *6*, 34-39.
32. Sun, Y. J.; Huang, X.; Soh, S., Solid-to-Liquid Charge Transfer for Generating Droplets with Tunable Charge. *Angew. Chem. Int. Ed.* **2016,** *55*, 9956-9960.
33. Jin, Y.; Wu, C.; Sun, P.; Wang, M.; Cui, M.; Zhang, C.; Wang, Z., Electrification of water: From basics to applications. *Droplet* **2022,** *1*, 92-109.
34. Britannica, The Editors of Encyclopaedia. "electrostatic induction". Encyclopedia Britannica, 18 Dec. 2011, https://www.britannica.com/science/electrostatic-induction. Accessed 29 November 2022.
35. Lim, K. H.; Sun, Y.; Lim, W. C.; Soh, S., Charging Organic Liquids by Static Charge. *J. Am. Chem. Soc.* **2020,** *142*, 21004-21016.
36. Wang, H.; Xiong, X.; Yang, L.; Cui, J., Droplets in soft materials. *Droplet* **2022,** *1*, 110-138.
37. Zhang, Y.; Hou, X., Liquid-based materials. *National Science Open* **2022,** *1*, 20220035.
38. Wang, F.; Liu, M.; Liu, C.; Zhao, Q.; Wang, T.; Wang, Z.; Du, X., Light-induced charged slippery surfaces. *Sci. Adv.* **2022,** *8*, eabp9369.
39. Zhang, Y.; Han, Y.; Ji, X.; Zang, D.; Qiao, L.; Sheng, Z.; Wang, C.; Wang, S.; Wang, M.; Hou, Y.; Chen, X.; Hou, X., Continuous air purification by aqueous interface filtration and absorption. *Nature* **2022,** *610*, 74-80.
40. Li, A.; Li, H.; Li, Z.; Zhao, Z.; Li, K.; Li, M.; Song, Y., Programmable droplet manipulation by a magnetic-actuated robot. *Sci. Adv.* **2020,** *6*, eaay5808.
41. Savage, A., Pyroelectricity and spontaneous polarization in LiNbO3. *J. Appl. Phys.* **1966,** *37*, 3071-3072.
42. Tang, X.; Li, W.; Wang, L., Furcated droplet motility on crystalline surfaces. *Nat. Nanotechnol.* **2021,** *16*, 1106-1112.
43. Tang, X., Multifunctional droplet‐surface interaction effected by bulk properties. *Droplet* **2023,** *2*, e38.
44. Jin, Y.; Xu, W.; Zhang, H.; Zheng, H.; Cheng, Y.; Yan, X.; Gao, S.; Wang, D.; Zi, Y.; Zhou, F.; Wang, Z., Complete Prevention of Contact Electrification by Molecular Engineering. *Matter* **2021,** *4*, 290-301.
45. Banks, H. T.; Sutton, K. L.; Clayton, W.; Bocharov, G.; Roose, D.; Schenkel, T.; Meyerhans, A., Estimation of cell proliferation dynamics using CFSE data. *Bull. Math. Biol.* **2011,** *73*, 116-150.

46. Elbuken, C.; Glawdel, T.; Chan, D.; Ren, C. L., Detection of microdroplet size and speed using capacitive sensors. *Sens. Actuators A: Phys.* **2011,** *171*, 55-62.

Figures

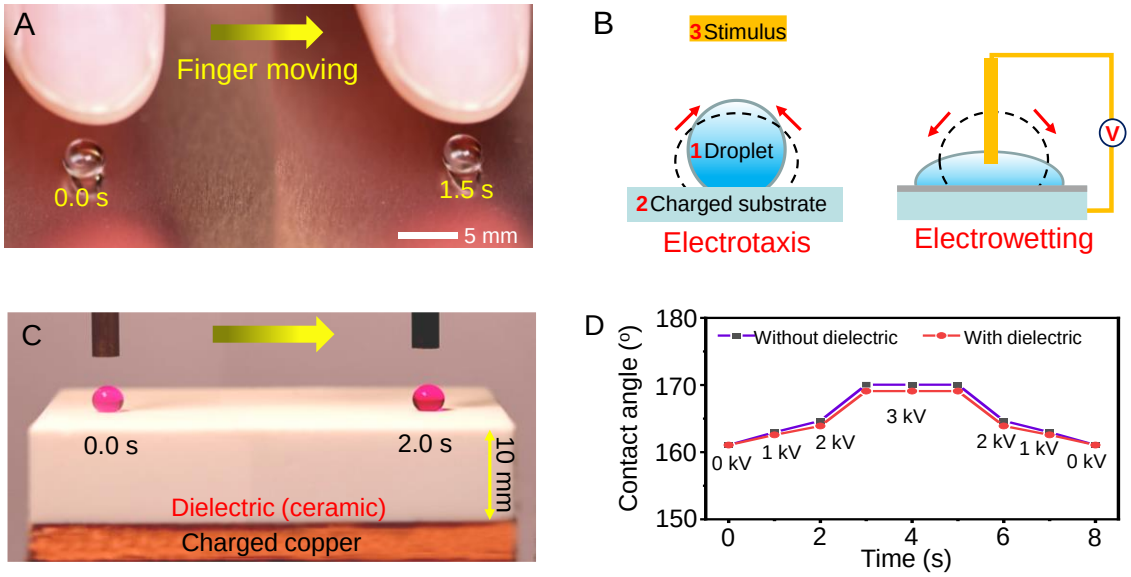

Figure 1. Droplet electrotaxis and its configuration. (A) Optical image showing the superimposed trajectory of water droplet on the charged superhydrophobic copper surface with the human finger moving. Here, the copper substrate acquires the charges from an electrostatic power supply. (B) Configuration comparison of droplet electrotaxis and traditional electrowetting. There are three key elements for droplet electrotaxis, including droplets (labeled as 1), charged substrates (labeled as 2), and external stimuli (labeled as 3). Electrotaxis induces the droplet to bead up, whereas electrowetting induces the droplet to spread, as denoted by the dashed lines and red arrows. (C) Electrotaxis motion of a water droplet on an additional dielectric layer (alumina ceramic with a thickness of 10 mm) supported by the charged copper substrates. (D) Contact angle of a water droplet (~ 7 μL) with electrotaxis on the substrates in the presence and absence of the dielectric layer (ceramic with a thickness of 10 mm). Here, various values of electrostatic voltages, output by an electrostatic power supply, are used to charge the substrates.

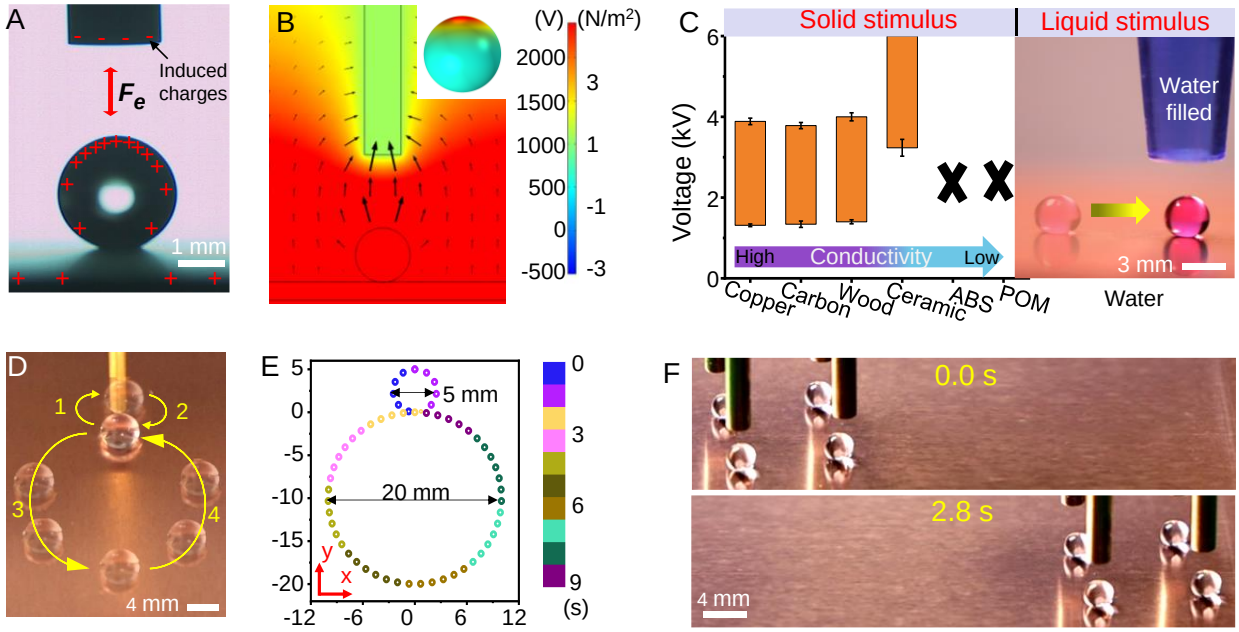

Figure 2. Mechanism of droplet electrotaxis, and electrotaxis-enabled droplet manipulation. (A) Schematic charges distribution in an optical image of droplet electrotaxis. The charges in droplets and substrates induce the generation of opposite polarity of induced charges in stimulus, generating an attractive electrostatic force, F_e . (B) Numerical simulation for the droplet electrotaxis. The external stimulus affects the distribution of the electric field around the droplet, thereby imposing an electrostatic attraction on the droplet. The inset shows the distribution of Maxwell stress tensor exerting on the droplet, and the red area denotes the stronger tensor on the top of the droplet. The left and right values of the color bar indicate the electric intensity in the figure and the Maxwell stress tensor in the inset, respectively. (C) The solid and liquid stimulus for the droplet electrotaxis. Left part: comparison of solid stimulus rods made of different materials in the aspect of voltage range for the electrotaxis motion of droplet (~7 μL). Right part: optical image for the electrotaxis of water droplet (red colored) in response to the liquid stimulus (blued colored water). The sign "X" means that the corresponding materials, *i.e.*, ABS, and POM, cannot trigger the droplet electrotaxis. The diameter of used solid stimulus rods is 3 mm, and the distance between stimulus rods and the charged substrate is 5 mm. (D) Superimposed trajectory of a water droplet moving along the circular tracks with a small diameter (5 mm) and larger diameter (20 mm). The numbered yellow lines denote the direction of droplet motion. (E) The time-evolved x–y position of the water droplet in (D). (F) The electrotaxis motion of droplet arrays.

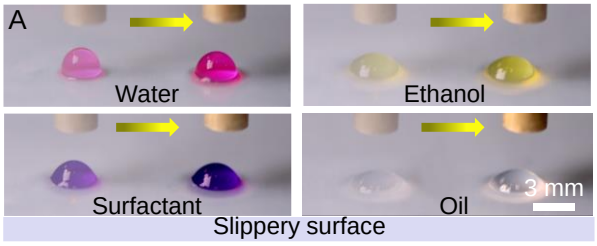

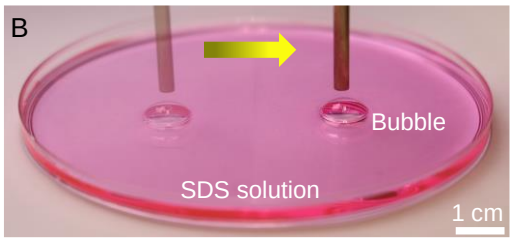

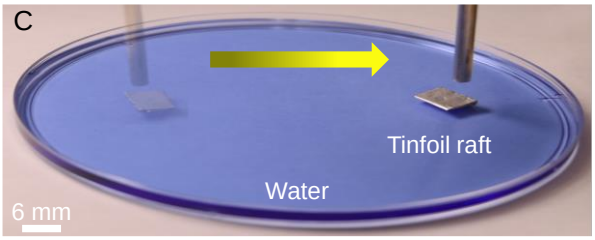

D Droplet-substrate interfaces	
Liquid-solid	√
Liquid-liquid	√
Gas-liquid	√
Solid-liquid	√
Liquid-solid (in liquid)	√

Figure 3. The generality of the droplet electrotaxis. (A) Optical images showing the electrotaxis of four droplets, including water, ethanol, surfactant (10 wt.% sodium dodecyl sulfate aqueous solution), and oil. Here, the lubricant-infused slippery surface offers a low drag force of liquid-liquid interface for the motion of droplets regardless of their viscosity and surface tension. (B) Electrotaxis motion of air bubble on the surface of charged SDS aqueous solutions. The utility of the SDS solution aims to promote the generation and stabilization of the bubble. (C) Electrotaxis motion of solid tinfoil rafted on charged water pool. The reason for choosing the tinfoil raft is based on its floating capacity on the liquid surface. (D) The list of droplet-substrate interfaces that are applicable to the droplet electrotaxis.

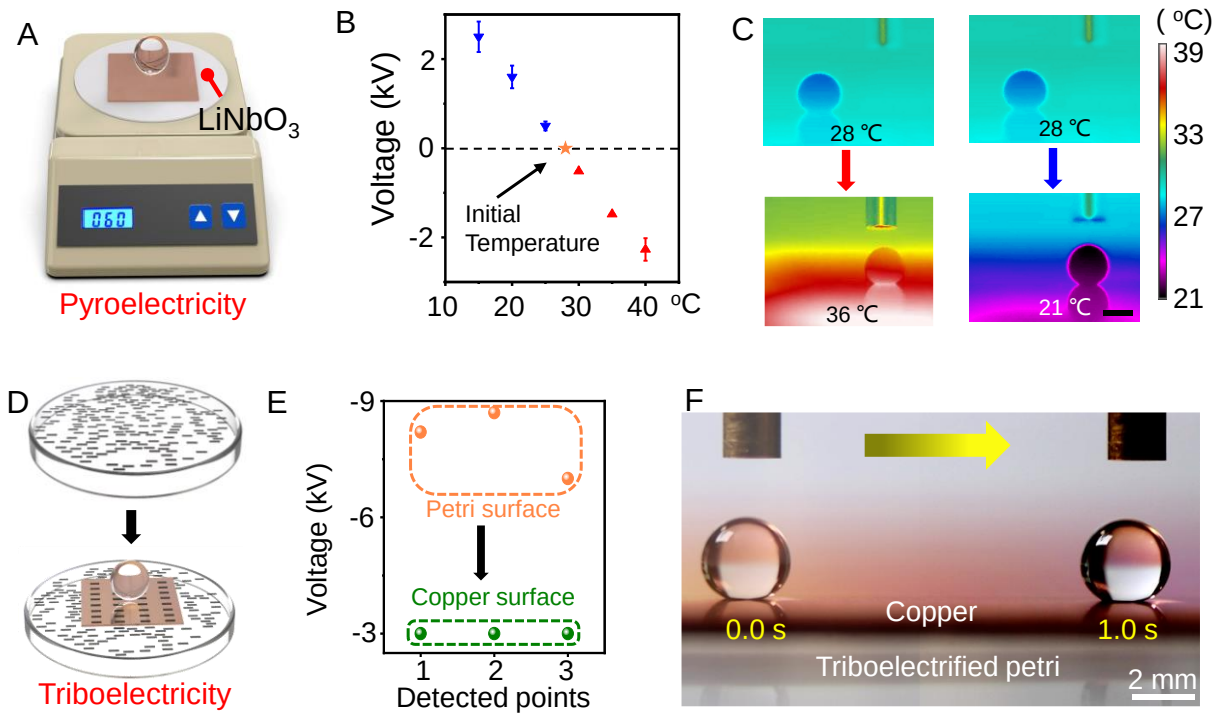

Figure 4. Diverse charge sources for droplet electrotaxis. (A) Schematic diagram of the design that harnesses the pyroelectricity to drive droplet electrotaxis. The pyroelectric effect of $LiNbO_3$ is activated by the underlying temperature controller. (B) The surface voltage of $LiNbO_3$-supported copper surface as a function of temperature. Temperature increase and decrease result in the generation of negative and positive voltage on surfaces, respectively. (C) Infrared images for the electrotaxis motion of droplet on $LiNbO_3$-supported copper surface by increasing or decreasing temperature. The scale bar is 3 mm. (D) Schematic diagram for the transformation of triboelectric charges from randomly distributed on plastic petri dish surface to uniformly distributed on the conductive metal substrate. Here, the utility of uniformly distributed charges on copper surface aims to denote its identical surface voltage. (E) The surface voltages of randomly selected three points on the triboelectrified petri surface (orange color) and the metal surface (olive color). (F) Optical time-lapse trajectory of droplets moving on superhydrophobic copper surface powered by the triboelectrified petri dish.

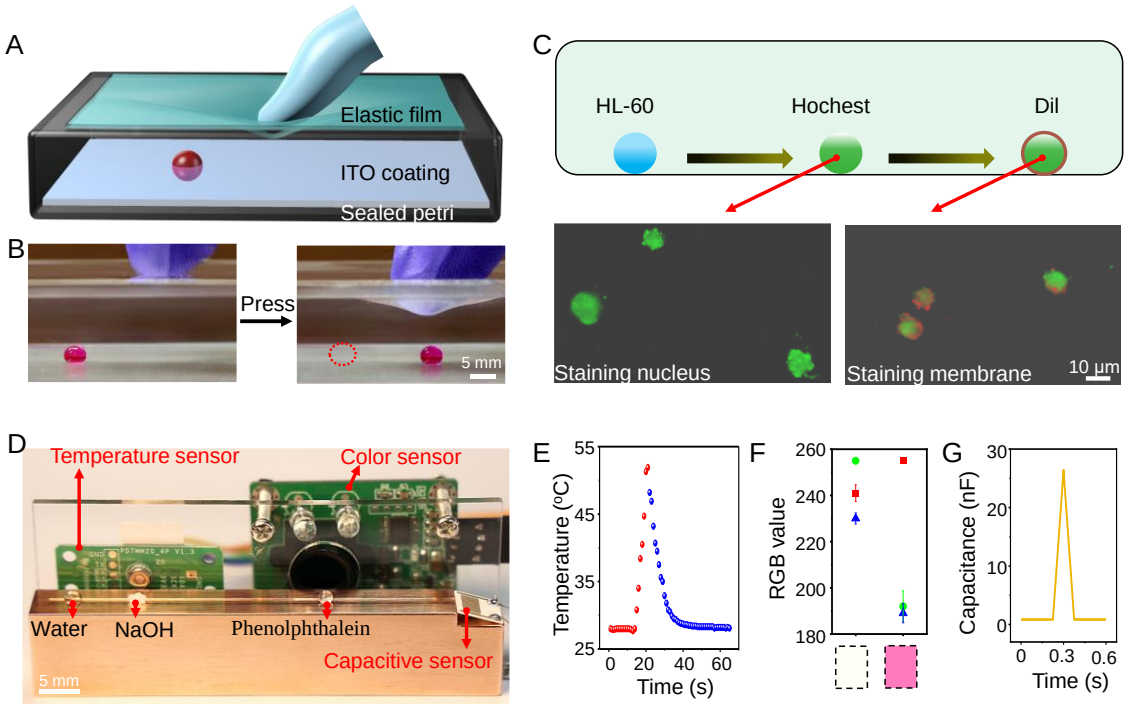

Figure 5. Application demonstration of the droplet electrotaxis. (A) Schematic diagram of enclosed droplet electrotaxis system fabricated with a skeleton of a petri dish. The upper elastic film with high resilience allows its momentary deformation and recovery by exerting and withdrawing external press force. The ITO coating is deposited on the bottom inner surface of the petri dish and then treated to be superhydrophobic, aiming to enhance the driving force for the droplet electrotaxis. The thickness of the elastic film is 100 μm. (B) Optical image showing the electrotaxis of red-colored water droplet perceiving the deformation of the elastic film. (C) Diagram for the cell staining in an enclosed electrotaxis system, and corresponding fluorescence images. The droplet containing cells of HL-60 is firstly transported to merge with the droplet containing Hochest to stain the nucleus. Next, the droplet further merges with the droplet containing Dil to stain the cell membrane. (D) Optical images of electrotaxis-based droplet information-recording integration. Such integration includes temperature sensor, color sensor, and capacitive counting sensor, allowing the information record for the droplet transported on the track of the copper substrate. (E-G) The output results of sensors. (E) The temperature change during the reaction of water droplet and sodium hydroxide powder. (F) RGB (red, green, blue) values of the droplet containing phenolphthalein before and after reaction with the sodium hydroxide aqueous droplet, and the corresponding color showed in the low part. (G) The capacitance changes when the droplet slides on the interdigital electrode that connects with the high-precision multimeter.